IEEE Access
Multidisciplinary | Rapid Review | Open Access Journal

Received August 4, 2019, accepted August 25, 2019, date of publication September 5, 2019, date of current version September 20, 2019.

Digital Object Identifier 10.1109/ACCESS.2019.2939542

Automatic Segmentation of the Left Ventricle From Cardiac MRI Using Deep Learning and Double Snake Model

YIHUA LAN[1,2] **AND RENCHAO JIN**[1,3]

[1]School of Computer Science and Technology, Huazhong University of Science and Technology, Wuhan 430074, China
[2]School of Computer and Information Technology, Nanyang Normal University, Nanyang 473061, China
[3]Key Laboratory of Education Ministry for Image Processing and Intelligence Control, Wuhan 430074, China

Corresponding author: Renchao Jin (jrc@hust.edu.cn)

This work was supported in part by the National Natural Science Foundation of China under Grant 81671768 and Grant 61401242, and in part by the WoLong Scholar Project at Nanyang Normal University.

ABSTRACT The left ventricle segmentation (LVS) is of great important for the evaluation of cardiac function. This study aimed to establish new segmentation algorithms that can enhance the accuracy and robustness of automatic LVS on magnetic resonance images. The datasets involved 45 subjects, including 12 heart failure patients with ischemia, 12 heart failure patients without ischemia, 12 hypertrophy patients and 9 normal individuals. The experiments consisted of three important steps. At first, deep learning was employed for the coarse LVS on myocardial images. Next, a double snake model was applied to assess the endo- and epi-cardial boundaries. Finally, the optimal epicardial boundary was obtained by adopting radial region growing method. Additionally, the performance of the developed LVS method was evaluated by the previously established software. Furthermore, the developed LVS method was validated by applying the datasets of 45 subjects. The results showed that the good contours, overlapping dice metric and average perpendicular distance of both epi- and endo-cardial contours were approximately 97%, 0.97 and 1.8 mm respectively. The regression coefficient and coefficient of determination between the proposed method and clinical experts were 0.96 and 1.039, respectively for ejection fraction, while 0.92 and 0.994 for left ventricle mass. These findings reveal that the developed method can enhance the accuracy and robustness of LVS. This novel LVS approach exhibits outstanding performance and possesses promising potential to increase the reliability of computer-aided imaging detection system for cardiovascular disease.

INDEX TERMS Convolutional neural network, snake model, left ventricle segmentation, magnetic resonance imaging, cardiac functional analysis.

I. INTRODUCTION

Cardiovascular disease is the number one cause of mortality worldwide, which has emerged as the most serious health problem [1], [2]. Assessment of the left ventricle segmentation (LVS) has gained increasing attention, as it allows the direct measurement of essential parameters including myocardial mass, end-diastolic volume and ejection fraction. Typically, LVS is carried out manually by highly experienced clinicians. However, the process of manual LVS is time-consuming and tedious, and its reproducibility is relatively low, resulting in large intra- and inter-observer variability [3]. Thus, it is necessary to establish a novel automatic extraction method of the left ventricular from MRI segmentation. Although considerable efforts have been devoted to the establishment of automatic LVS, this remains a difficult clinical problem. There have been extensive researches to overcome the potential shortcomings of LVS, such as dynamic programming (DP) [4]–[6], snake models [7]–[9], thresholding [10], region growing [11], pixel classification [12]–[14]. A comprehensive review of LVS techniques has been described previously [15]. Among the above-mentioned approaches, the snake model has been commonly used to solve a wide range of segmentation issues, including LVS. Indeed, the theoretical framework of this model remains similar with that invented over the past three decades [16], [17]. An energy minimizing is applied to obtain an evolution equation (explicit or implicit) according to the image contents. However, some difficulties may be encountered for the current methods of LVS. First, the

The associate editor coordinating the review of this manuscript and approving it for publication was Huimin Lu.

epi- and endo-cardial contours may have the same shapes, thus resulting in greater complexity during the extraction of myocardial boundaries. Second, considering the relatively similar edges between epi- and endo-cardial contours, the current methods can confuse the subsequent contour as the initial boundary. Third, unforeseen failure for cardiac image segmentation is inevitable, including the unexpected changes in intensity distribution along the peripheral vessels of myocardial infarction patients. Over the past decades, deep learning methods (i.e. Convolutional Neural Networks [CNNs]), are often adopted for medical image computing [18] with substantial success. CNNs have been successfully adopted in the areas of image processing and computer vision [18]–[21]. A previous study has employed CNNs to identify the left ventricle, and subsequently used a Stacked AutoEncoder to infer the shape of the left ventricle [22]. To enhance the accuracy and reliability of LVS, they establish a deformable model that consists of prior shape information and energy terms. By comparing with the datasets of MICCAI 2009 LVS challenge, an outstanding performance was obtained for the endocardial contours [23]. In view of this, we aimed to establish a hybrid approach based on deep learning and double snake model for determining LVS in a large-scale population assessment. Segmentation of the left ventricle myocardial boundaries was performed via CNNs, and the results were refined for both epi- and endo-cardial contours. Such application is assisted by the CNNs data-driven localization of the myocardial boundaries in order to provide a robust and reliable measurement of epi- and endo-cardial edges. By integrating CNNs and snake model, more accurate localization and obvious morphological characteristics LVS can be achieved. The present research is structured as follows. In the Methodology section, the developed modelling-simulation-analysis workflow is described in detail. Next, in the Results and Validation section, the performance analysis and comparison showed that our proposed method is superior to previously published methods. Finally, a valid conclusion is drawn and future research directions are provided.

II. MATERIALS AND METHODS

A. DATASET

The datasets employed here were short axis cardiac cine MRI images published online [1] by MICCAI grand challenge. A total of 45 subjects were enrolled in this study, including heart failure patients with ischemia (HF-I; n = 12), heart failure patients without ischemia (HF-NI; n = 12), hypertrophy patients (HYP; n = 12) and normal individuals (N; n = 9) Their cardiac MRI images were acquired during breath-hold sessions lasting for 10 to 15 s with a temporal resolution of 20 cardiac phases per cardiac cycle. Six to twelve SAX images were acquired from the atrioventricular ring to the apex (FOV = 320 mm × 320 mm; thickness = 8∼10 mm; matrix = 256 × 256).

[1] http://sourceforge.net/projects/cardiac-mr/files/

B. ANALYTICAL FRAMEWORK FOR SEGMENTATION ALGORITHM

The present method employed the discriminative features of CNNs for the purpose of automated heart localization in the cardiac MRI image. The entire work-flow of the segmentation algorithm consisted of three steps Fig.1. Firstly, the ground truth and short axis images were used to construct and train the CNN model. Next, short axis images were extracted for each new case by using the CNN parameters derived from the initial step in order to compute the coarse myocardial segmentation. Lastly, a constrained region was built according to the coarse contours of LV, in order to obtain an appropriate epicardial contour for the final dynamic programming-based segmentation method.

The overall procedure of LVS involving a collection of image processing methods is shown in in Fig.1. The algorithms began by identifying the ROI in the cardiac MRI slices. Then, the improved snake model was applied to extract blood pool activities. After that, topological stable-state thresholding approach was used to obtain refined endocardial contours. For epicardial contour extraction, an edge map was determined from the gradient images, followed by analysis with multi-constrained dynamic programming technique. The following sections describe the proposed LVS method in details.

1) STEP I: DEEP CNNs

In CNNs, the neuronal cells are weakly attached to the neighboring cells through weights, thus stacking across the images. This enables CNNs with invariant features and accelerates training process in comparison with the fully connected neural network [24]. Another advanced feature of CNNs is representation learning, in which the weights are associated with the optimal and automatic feature learning detectors. Over the past five years of applications, CNNs have been demonstrated to exhibit unrivaled performance [25]. Due to their great achievement, CNNs are commonly applied to medical image processing [26].

Different types of CNN architectures are designed to fulfill specific aims. In this study, we employed SegNet, an CNN-based encoder-decoder approach [27]. The parameters of SegNet, with stacking of 17 convolutional layers, are presented in Fig. 2. The first 4 convolution layers were consisted of batch normalization (BN) and Rectified Linear Unit (ReLU). The addition of 4 MaxPool layers allowed higher-layer representations to be invariant to small translations of the input. The 4 upscale layers up-sampled their input feature maps and integrated them with the corresponding encoder feature map to generate the input to the next decoder [28].

SegNet has been well-trained to segment the MRI images in order to assess the blood pool and myocardial regions. Given the spatial relationship among left ventricle slice images, the left ventricle blood pool and myocardial regions on the top and bottom of slice images are not far away from those in the middle of slice images. Base on SegNet data, the location of blood pool and myocardium can be detected

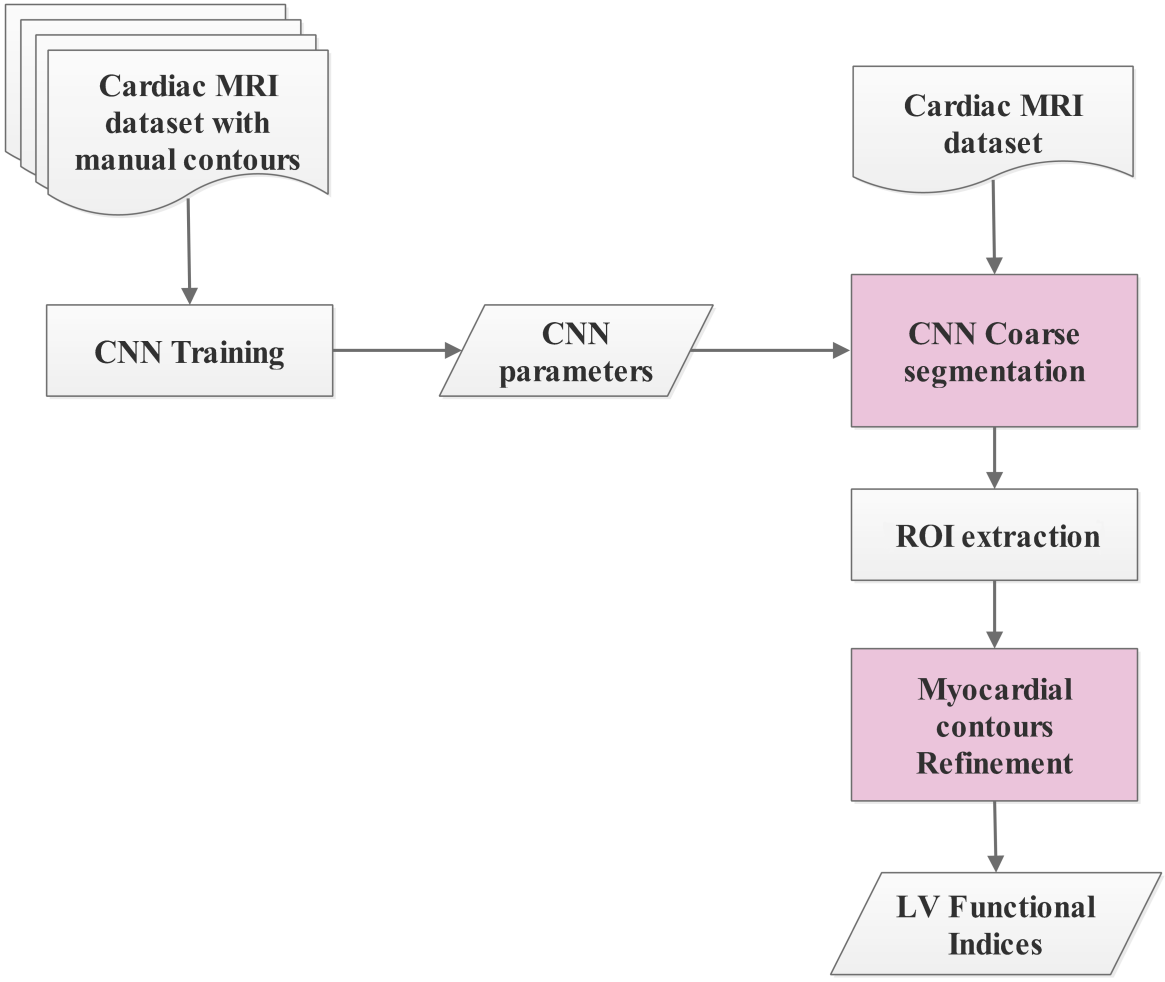

FIGURE 1. Schematic diagram depicting the steps during LVS analysis.

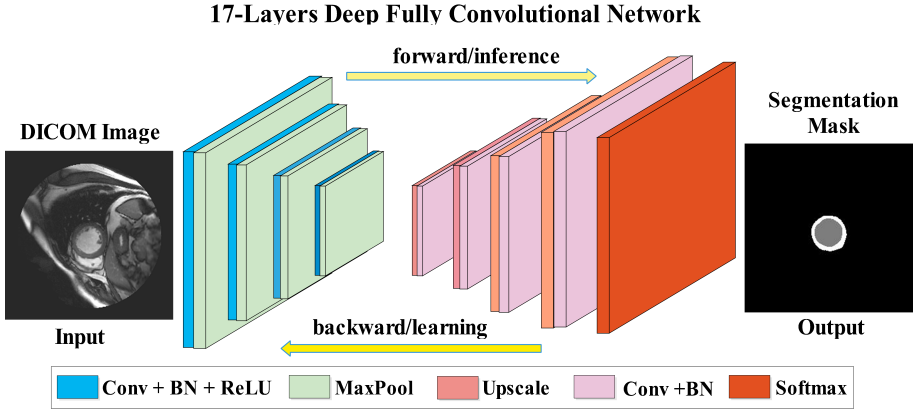

FIGURE 2. Architectural design and construction of the CNNs. BN: batch normalization; ReLU(x) = max (0, x).

from the slice images in both end-systole and end-diastole phases.

The segmentation results obtained from SegNet were refined for myocardial contours. Moreover, a centered, fixed rectangular ROI is pointed out at the middle position of the resulting endo-cardial contours (Fig. 3). Subsequently, the ROI is converted into rectangle shape image through polar transform, with center point as a pole (Fig. 4(A) and 4(B)).

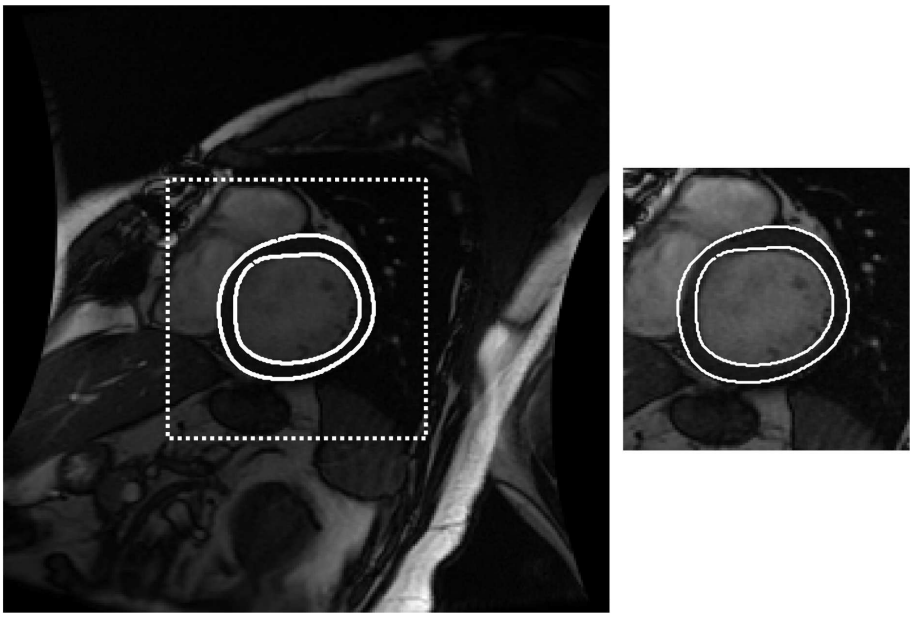

FIGURE 3. Original image and ROI. The right and left images represent original CMR depicting epi- and endo-cardial contours generated by CNNs, respectively. Solid white curves highlight both epi- and endo-cardial contours.

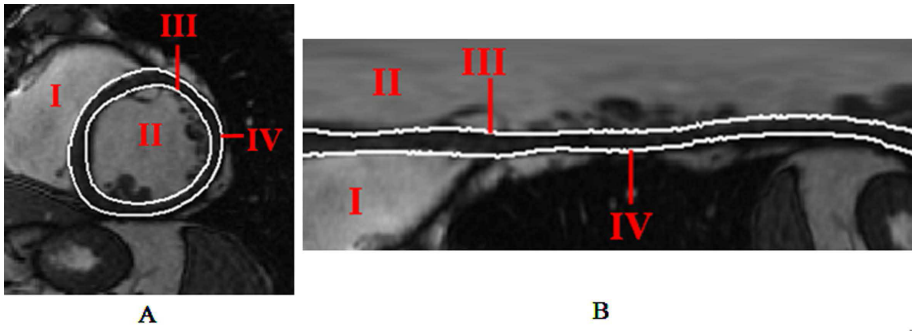

FIGURE 4. Structure of the left ventricle (I. blood pool of the right ventricle; II. blood pool of the left ventricle; III endocardial contour; IV epicardial contour). (a) ROI; (b) transformed rectangular image via polar transform.

2) STEP 2: SNAKE MODEL CONSTRUCTION

Given the ROI in polar coordinate system, a curve L that is driven by edge force, balloon force and curvature force was identified [29], [30]. The proposed snake model is as follows:

$$L_{t+1} = L_t + \gamma(\alpha_E * F_E + \alpha_B * F_B - \alpha_C * F_C) \quad (1)$$

where F_E is the edge force, F_B denotes the balloon force, F_C represent curvature force. $\alpha_E = 15$, $\alpha_B = 5$ and $\alpha_C = 0.1$ are image modality dependent. γ constant is equal to 0.75 multiply by the smallest distance between two nodes and then divided by the greatest force. It is further reduced to the lowest value of 0.05 multiply by the normalization.

The proposed edge force F_E was separated into 2 variants, as shown in Fig. 5. The deformable model of concordant edge force was engaged with only a black-white transition, while that of discordant edge force was engaged with different types of transition (i.e. white-black or black-white). Input images were generated by the edge detection, in accordance with the polar radius direction. The edge force F_E is calculated as follows:

$$\begin{aligned} concordantedgeforce: \quad & F_E = I * f * s \\ discordantedgeforce: \quad & F_E = |I * d * s| * d \\ & f = \begin{bmatrix} 1 \\ -2 \\ 1 \end{bmatrix}; \quad s = \begin{bmatrix} 0.25 \\ 0.5 \\ 0.25 \end{bmatrix}; \\ & d = \begin{bmatrix} -1 \\ 0 \\ 1 \end{bmatrix} \end{aligned} \quad (2)$$

where I represents the input image, $*$ delineates image convolution, and f, d and s denote small edge-detecting, derivate and small directional smoothing filters, respectively.

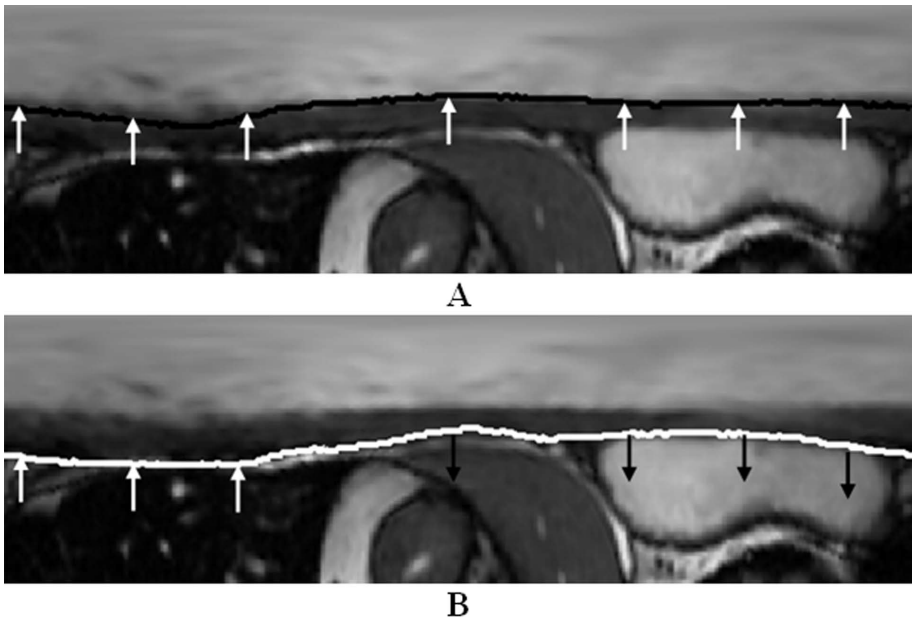

FIGURE 5. Representative images for concordant edge and discordant edge forces. (a) concordant edge force; (b) discordant edge force.

The inflating balloon force used in this research is image dependent, and is calculated as follows:

$$Endocardial \quad F_B = (I - 0.5 * \lambda) \tag{3}$$

$$Epicardial \quad F_B = (e^{-(I-\lambda)^2} - 0.5) \tag{4}$$

where λ is an estimated image intensity of the input image I. The internal force of the snake model is curvature force, in order to ensure a smooth model surface (in the short axis plane). It is derived from the calculation of the curvature on the model surface.

$$F_C = \kappa \tag{5}$$

where κ is the curvature of the deformable model curve L. The coarse endocardial contour of CNN segments is considered as the first contour for snake model, and thus the endocardial contour can be derived iteratively according to the Equation.1.

3) STEP 3: CALCULATION OF THE EPICARDIAL CONTOUR

The procedure of epicardial contour extraction is similar to endocardial boundary extraction with regards to the polar system used. However, only specific locations are available for identifying the edge points of epicardial. Therefore, we employed region growing method to find the epicardial contour. To locate the epicardial contour, the epicardial contour of CNN segments was considered as the first contour for snake model according to the 1 and a coarse epicardial edge could be obtained Fig.6(A). The search for the edge points of epicardial was initiated from the endocardial contour. The endo- and epi-cardial contours extracted by snake model, together with the epicardial contour regions obtained from the preceding slice images, were used to construct a binary mask, in order to define the search range for the edge points of epicardial contour in the following region growing method Fig.6(B).

In this study, radial region growing method was employed to extract the epicardial contour of the left ventricle. At present, the radial region growing has been recognized as single direction region growing method, originating from the endocardial contour. This approach utilizes a threshold value in the detection of muscle activity, and it determines both intensity value and binary mask to identify the stopping criterion. To ensure a smooth contour that adapts the epicardial surface, the first edge of epicardial was refined by 1D FFT (fast Fourier transform). Subsequently, the edge point was inversely transformed to determine both epi- and endocardial contours. Furthermore, 1D FFT and Bezier curve fitting methods [31] were applied to smooth the contours. The formula for 1D FFT approach is expressed as follows:

$$\begin{cases} x^* = IFFT(H * FFT(x)) \\ y^* = IFFT(H * FFT(y)) \end{cases} \tag{6}$$

where x, y represent the Cartesian coordinates of the edge points; IFFT denotes the inverse FFT;H indicates a low pass filter.

C. EVALUATION OF THE SEGMENTATION MODEL

In the present study, we tested 45 datasets reported by the MICCAI Clinical Image Segmentation Grand Challenge Workshop. The same assessment software used in that report [32] was adopted in this study. The data and assessment software can be retrieved freely, which allow investigators to develop and evaluate their algorithms efficiently

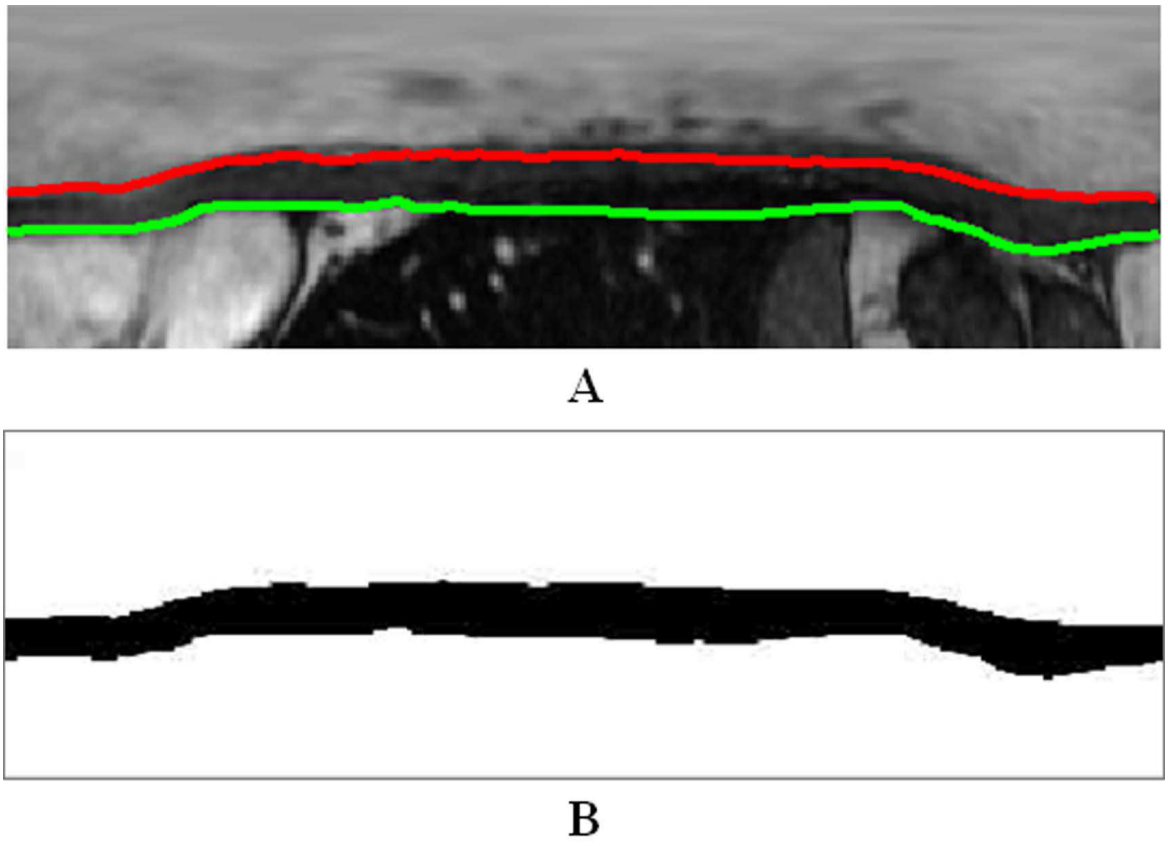

FIGURE 6. Construction of a region constrained mask: (A) endo- and epi-cardial contour, (B) a binary region constrained mask.

TABLE 1. LVS outcomes of the 45 cases.

		Good contours (%)		Average perpendicular distance (mm)		Overlapping dice metric		Ejection fraction (%)		Left ventricular mass (g)	
Group	Cases	Endo	Epi	Endo	Epi	Endo	Epi	Auto	Expert	Auto	Expert
HF-I	12	97.52	98.97	1.80	1.82	0.97	0.98	26.33	25.61	132.35	132.52
HF-NI	12	96.75	96.57	1.81	1.87	0.96	0.97	30.99	28.86	144.43	128.47
HYP	12	95.12	98.09	1.85	1.86	0.94	0.95	65.01	60.93	103.46	103.76
N	9	98.91	98.02	1.77	1.82	0.98	0.97	64.19	58.26	88.82	86.53
Total	45	97.08	97.91	1.81	1.84	0.96	0.97	45.46	42.42	119.16	114.57
Overall	45	97.50±6.75		1.83±0.49		0.97±0.03					

Endo, endocardial contours; epi, epicardial contours; HF-I, heart failure patients with ischemia; HF-NI, heart failure patients without ischemia; HYP, hypertrophy patients; N, normal subjects.

and impartially. Indeed, numerous parameters were used in the model, including the good contours, overlapping dice metric, average perpendicular distance, ejection fraction and left ventricle mass.

The ground truth of the left ventricle was extracted from the datasets by experienced clinicians. The contours were considered good if their mean distance from the ground truth was less than 5 mm. The calculation for the values of good contours, overlapping dice metric and average perpendicular distances are as follows. Good contours (%) = the number of good contours / the total number of all tested contours. Overlapping dice metric = the region overlapping proportion between automatic delineation and ground truth. Average perpendicular distance equals to the distance between the automatically segmented contour and the corresponded to manual segmented contour / total contour points. Besides, different approaches have been developed to calculate the volume of the left ventricle, in which both ejection fraction and the left ventricle mass are essential parameters for cardiac function evaluation [33]. Specifically, the left ventricle mass and are delineated as follows:

$$LVM = (V_{epi}^{ED} - V_{end}^{ED}) * 1.05 \tag{7}$$

$$EF = \frac{(V_{end}^{ED} - V_{end}^{ES})}{V_{end}^{ED}} * 100\% \tag{8}$$

TABLE 2. Comparison of the segmentation performance between the proposed algorithm and other state-of-the-art methods.

	Method	Proposed	Ngo, Lu and Carneiro (2017) [35]	Avendi et al. (2016) [22]	Ngo and Carneiro. (2014) [36]	Queiros et al . (2014) [37]	Hu et al. (2013) [6]	Constantinides et al. (2012) [38]
case	(#)[1]	45	45	30	30	45	45	45
Good (%)	Endo	97.08 (7.0)	94.55 (9.31)	96.69 (5.7)	1.95 (0.48)	92.70 (9.5)	91.06 (9.4)	80 (16)
	Epi	97.91 (6.5)	92.49 (15.31)	-	1.95 (0.48)	95.4 (9.6)	91.21 (8.5)	71 (26)
Dice metric	Endo	0.96 (0.03)	0.88(0.04)	0.94 (0.02)	0.89 (0.03)	0.90 (0.05)	0.89 (0.03)	0.86 (0.05)
	Epi	0.97 (0.02)	0.93 (0.02)	-	-	0.94 (0.02)	0.94 (0.02)	0.91 (0.03)
APD (mm) [2]	Endo	1.81 (0.35)	2.22 (0.46)	1.81 (0.44)	2.26 (0.46)	1.76 (0.45)	2.24 (0.40)	2.44 (0.56)
	Epi	1.84 (0.63)	2.04 (0.55)	-	-	1.80 (0.41)	2.19 (0.49)	2.80 (0.71)
Conformity	Endo	0.92	0.73	0.87	0.75	0.78	0.75	0.67
	Epi	0.94	0.85	-	-	0.87	0.87	0.80

[1] Total number of tested datasets. [2] APD: average perpendicular distance.

where V_{epi}^{ED} and V_{end}^{ED} denote the epi- and endo-cardial volumes, respectively, during end-diastole phase, while V_{end}^{ES} stands for the endocardial volume during end-systole phase.

III. RESULTS

A. LVS OUTCOMES OF THE 45 CASES

In the present study, a total of 45 cases were included and analyzed in the model. Table 1 shows the comparison between automatic segmentation and ground truth. Our results demonstrated that the overall good contours, overlapping dice metric and average perpendicular distance of epi- and endocardial contours were approximately 97%, 1.8 mm and 0.97, respectively. In addition, the computation time of LVS was analyzed by Matlab code (Mathworks) using pentium Ddual-core 2.60 GHz hardware. Among the 45 cases, the average computation time for reading DICOM slices and saving contour files was 58.98±11.49 seconds for each case. Moreover, the computation time was 3.26 seconds in average for assessing each image among the 45 cases. As shown in Table 2, our current approach exhibited a great advantage over the other state-of-the-art methods by comparing good contours, overlapping dice metric, average perpendicular distance and conformity [34] using the same database.

B. REGRESSION AND BLAND-ALTMAN ANALYSES

Regression and Bland-Altman analyses were used to determine the accuracy of our LVS method. The regression and Bland-Altman plots for the measurements of left ventricle mass and ejection fraction are presented in Fig. 7a-d. It was found that the regression coefficient for the measurement of ejection fraction was 1.0392, and the bias was 3.07 according to Bland-Altman plot Fig.(7(A) and 7(B)). Meanwhile, the slope of the left ventricle mass was 0.994, and the bias was 4.59 according to Bland-Altman plot. The coefficient of determination for ejection fraction and left ventricle mass were 0.96 and 0.92, respectively. Taken altogether, the proposed LVS method is quite accurate for measuring left ventricle mass and ejection fraction.

C. METHOD COMPARISON

Fig.8 shows the LVS outcomes of selected patients analyzed by our method and clinical experts. Red circles denote the contour drawn by clinical experts; while green circles represent the outputs from our method. Four groups of cases were tested in our experiments as mentioned above, and the four types of images were arranged in different rows (Fig.8). The 1st row is HF-I group, the 2nd row is HF-NI group, the third row is HYP group, and the last row is normal subjects. Two resultant images of end-systole phase (left) and end-diastole phase (right) are demonstrated for each case. Ground truth of the left ventricleą́s epicardial contour was neglected during end-systole phase, due to its unnecessity for measuring left ventricle mass and ejection fraction.

Fig.9 demonstrates a heart failure patient without ischemia (SC-HF- I-05). The outcomes of LVS were different between our approach and clinical experts. Red circles delineate the contours drawn by clinical experts, whereas green circles stand for our outputs. The images with odd numbers are from the end-systole phase, while those with even numbers belong to the end-diastole phase. Ground truth of the left ventricleą́ epicardial contours during end-systole phase was excluded by clinical experts, due to its unnecessity for measuring left ventricle mass and ejection fraction.

D. DISCUSSION

In the present study, an automatic LVS method is established for the evaluation of left ventricle volumes and functions in multi-slice short-axis MRI images. The proposed method incorporates a sequence of image segmentation techniques, such as snake model, thresholding and radial region growing. The findings demonstrate a highly promising performance of our method compared to others.

During LVS process, Otsu thresholding and Gaussian-mixture model have been commonly used to identify the location of the left ventricle blood pool. The effectiveness of Gaussian mixture model-based segmentation algorithms is largely dependent on the histogram of images and accuracy of the estimated model parameters [39]. For the Otsu

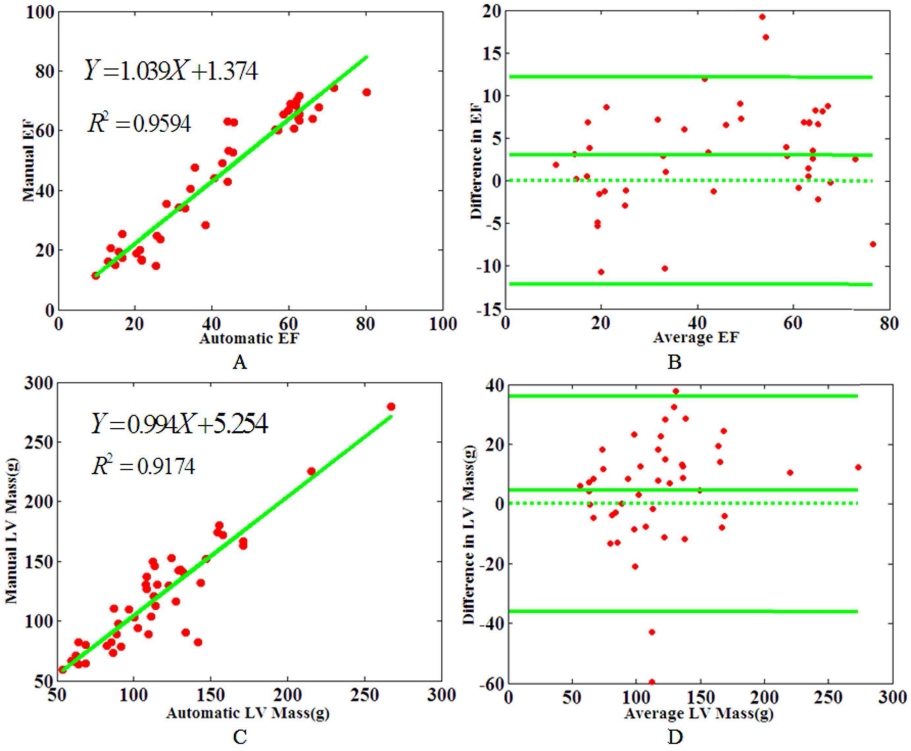

FIGURE 7. Regression curve and Bland-Altman plots for measuring ejection fraction and left ventricle mass. (A) Linear regression for the measurement of ejection fraction; (B) Bland-Altman plot for the measurement of ejection fraction; (C) linear regression for the measurement of left ventricular mass; and (D) Bland-Altman plot for the measurement of left ventricular mass.

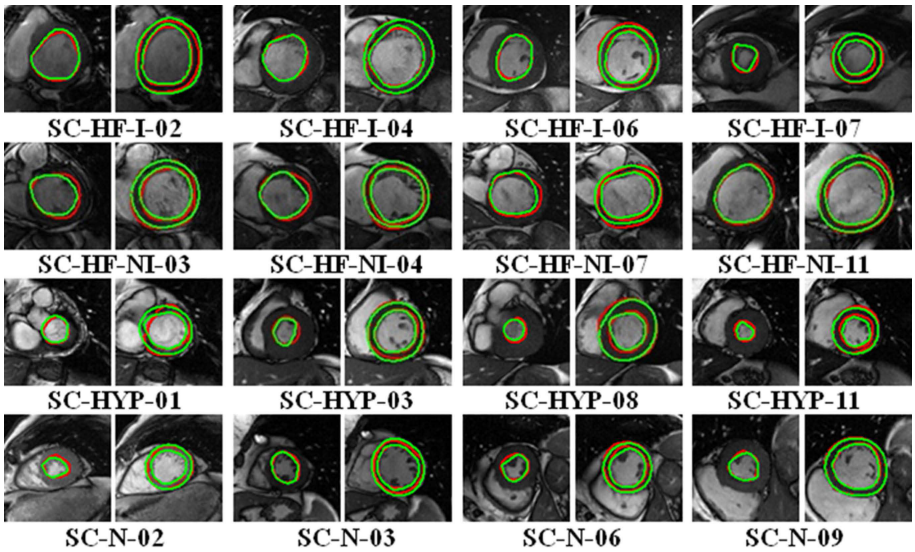

FIGURE 8. LVS outcomes of selected patients (cropped for better viewing). First row: Heart failure patients with ischemia (HF-I); second row: Heart failure patients without ischemia (HF-NI); third row: Hypertrophy patients (HYP); and last row: Normal subjects.

method [40], several segmentation errors may be resulted from the potential incorrect threshold, due to the larger variances of both object and background intensities compared to the mean difference [41], [42]. This study solves the above problem by deep learning and transforming the images into polar coordinates. Such approach is effective for conducting image segmentation in the polar coordinate system, and it has been adopted by few other studies [6], [43]. After transformation, it is one-way direction for snake model and radius region growing, which is easy to implement and time saving. In addition, the parameters of good contours, overlapping dice metric and average perpendicular distance were used

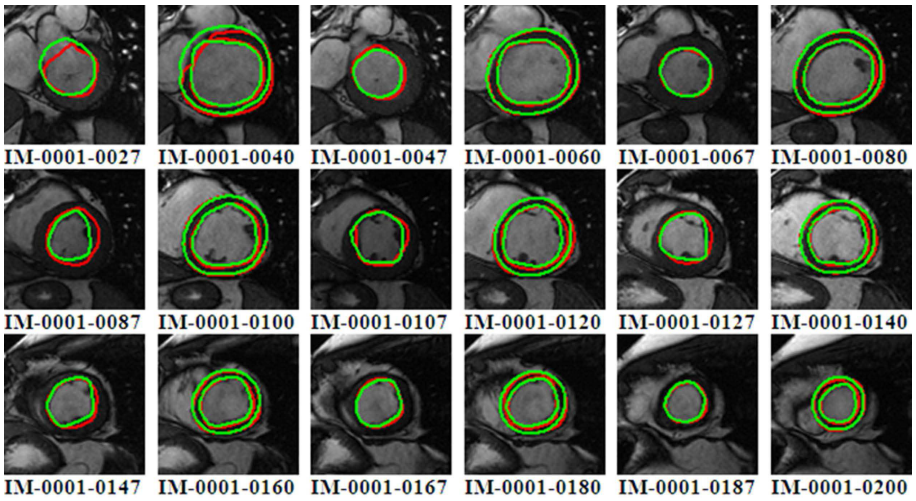

FIGURE 9. LVS outcome of a representative case (SC-HF-I-05) analyzed using the proposed method (cropped for better viewing).

to evaluated the performance of our LVS method. Moreover, the cardiac function parameters (i.e. ejection fraction and left ventricular volume) were assessed with regression and Bland-Altman analyses. Taken altogether, the findings reveal that the developed method exhibit higher accuracy and greater robustness compared to other methods.

IV. CONCLUSION

In this study, an automatic method has been established to segment the left ventricle on MRI. Experimental results on 45 cases demonstrate that our proposed LVS method generates more reliable findings compared to other methods. This novel LVS approach can be valuable for enhancing the reliability of computer-aided imaging detection system for cardiovascular disease. Despite that this method tend to be more reliable than previous methods, substantial challenges remained at few extreme cases, with regards to the overlapping of intensity distribution throughout the cardiac regions. Therefore, it is necessary to enhance the accuracy of LVS method and conduct addition researches on the right ventricle extraction in the near future.

REFERENCES

[1] E. J. Benjamin, S. S. Virani, C. W. Callaway, A. M. Chamberlain, A. R. Chang, S. Cheng, S. E. Chiuve, M. Cushman, F. N. Delling, and R. Deo, "Heart disease and stroke statistics-2018 update: A report from the American heart association," *Circulation*, vol. 137, no. 12, p. e67, 2018.

[2] C. Ricci, A. Wood, D. Müller, M. J. Gunter, A. Agudo, H. Boeing, Y. T. Van Der Schouw, S. Warnakula, C. Saieva, and A. Spijkerman, "Alcohol intake in relation to non-fatal and fatal coronary heart disease and stroke: Epic-cvd case-cohort study," *BMJ*, vol. 361, p. k934, May 2018.

[3] H.-Y. Lee, N. C. F. Codella, M. D. Cham, J. W. Weinsaft, and Y. Wang, "Automatic left ventricle segmentation using iterative thresholding and an active contour model with adaptation on short-axis cardiac MRI," *IEEE Trans. Biomed. Eng.*, vol. 57, no. 4, pp. 905–913, Apr. 2010.

[4] J.-Y. Yeh, J. C. Fu, C. C. Wu, H. M. Lin, and J. W. Chai, "Myocardial border detection by branch-and-bound dynamic programming in magnetic resonance images," *Comput. Methods Programs Biomed.*, vol. 79, no. 1, pp. 19–29, 2005.

[5] M. Üzümcü, R. J. van der Geest, C. Swingen, J. H. Reiber, and B. P. Lelieveldt, "Time continuous tracking and segmentation of cardiovascular magnetic resonance images using multidimensional dynamic programming," *Invest. Radiol.*, vol. 41, no. 1, pp. 52–62, 2006.

[6] H. Hu, H. Liu, Z. Gao, and L. Huang, "Hybrid segmentation of left ventricle in cardiac MRI using Gaussian-mixture model and region restricted dynamic programming," *Magn. Reson. Imag.*, vol. 31, no. 4, pp. 575–584, 2013.

[7] Y. Wang, Y. Wu, and Y. Jia, "Shape constraints for the left ventricle segmentation from cardiac cine mri based on snake models," in *Shape Analysis in Medical Image Analysis*. Cham, Switzerland: Springer, 2014, pp. 373–412.

[8] A. R. De Alexandria, P. C. Cortez, J. A. Bessa, J. H. da Silva Felix, J. S. De Abreu, and V. H. C. De Albuquerque, "pSnakes: A new radial active contour model and its application in the segmentation of the left ventricle from echocardiographic images," *Comput. Methods Programs Biomed.*, vol. 116, no. 3, pp. 260–273, 2014.

[9] M. R. Kaus, J. von Berg, J. Weese, W. Niessen, and V. Pekar, "Automated segmentation of the left ventricle in cardiac MRI," *Med. Imag. Anal.*, vol. 8, no. 3, pp. 245–254, Sep. 2004.

[10] H. Liu, H. Hu, X. Xu, and E. Song, "Automatic left ventricle segmentation in cardiac MRI using topological stable-state thresholding and region restricted dynamic programming," *Acad. Radiol.*, vol. 19, no. 6, pp. 723–731, 2012.

[11] S. Huang, J. Liu, L. C. Lee, S. K. Venkatesh, L. L. S. Teo, C. Au, and W. L. Nowinski, "An image-based comprehensive approach for automatic segmentation of left ventricle from cardiac short axis cine mr images," *J. Digit. Imag.*, vol. 24, no. 4, pp. 598–608, 2011.

[12] M. Lynch, O. Ghita, and P. F. Whelan, "Automatic segmentation of the left ventricle cavity and myocardium in MRI data," *Comput. Biol. Med.*, vol. 36, no. 4, pp. 389–407, 2006.

[13] C. M. S. Nambakhsh, J. Yuan, K. Punithakumar, A. Goela, M. Rajchl, T. M. Peters, and I. B. Ayed, "Left ventricle segmentation in MRI via convex relaxed distribution matching," *Med. Image Anal.*, vol. 17, no. 8, pp. 1010–1024, 2013.

[14] A. Eslami, A. Karamalis, A. Katouzian, and N. Navab, "Segmentation by retrieval with guided random walks: Application to left ventricle segmentation in MRI," *Med. Image Anal.*, vol. 17, no. 2, pp. 236–253, 2013.

[15] C. Petitjean and J.-N. Dacher, "A review of segmentation methods in short axis cardiac MR images," *Med. Image Anal.*, vol. 15, no. 2, pp. 169–184, 2011.

[16] M. Kass, A. Witkin, and D. Terzopoulos, "Snakes: Active contour models," *Int. J. Comput. Vis.*, vol. 1, no. 4, pp. 321–331, 1988.

[17] D. Adalsteinsson and J. A. Sethian, "The fast construction of extension velocities in level set methods," *J. Comput. Phys.*, vol. 148, no. 1, pp. 2–22, Jan. 1999.

[18] F. Zhang, B. Du, and L. Zhang, "Saliency-guided unsupervised feature learning for scene classification," *IEEE Trans. Geosci. Remote Sens.*, vol. 53, no. 4, pp. 2175–2184, Apr. 2015.
[19] W. Zhang, R. Li, H. Deng, L. Wang, W. Lin, S. Ji, and D. Shen, "Deep convolutional neural networks for multi-modality isointense infant brain image segmentation," *NeuroImage*, vol. 108, pp. 214–224, Mar. 2015.
[20] Y. Dong, B. Du, and L. Zhang, "Target detection based on random forest metric learning," *IEEE J. Sel. Topics Appl. Earth Observ. Remote Sens.*, vol. 8, no. 4, pp. 1830–1838, Apr. 2015.
[21] H. Hu, N. Pan, J. Wang, T. Yin, and R. Ye, "Automatic segmentation of left ventricle from cardiac MRI via deep learning and region constrained dynamic programming," *Neurocomputing*, vol. 347, pp. 139–148, Jun. 2019.
[22] M. R. Avendi, A. Kheradvar, and H. Jafarkhani, "A combined deep-learning and deformable-model approach to fully automatic segmentation of the left ventricle in cardiac MRI," *Med. Image Anal.*, vol. 30, pp. 108–119, May 2016.
[23] *MICCAI 2009 Segmentation Challenge*. Accessed: Sep. 24, 2009. [Online]. Available: http://smial.sri.utoronto.ca/LV_Challenge/Data.html
[24] J. Masci, A. Giusti, D. Ciresan, G. Fricout, and J. Schmidhuber, "A fast learning algorithm for image segmentation with max-pooling convolutional networks," in *Proc. IEEE Int. Conf. Image Process.*, Sep. 2013, pp. 2713–2717.
[25] A. Alzu'bi, A. Amira, and N. Ramzan, "Compact root bilinear CNNs for content-based image retrieval," in *Proc. Int. Conf. Image, Vis. Comput. (ICIVC)*, Aug. 2016, pp. 41–45.
[26] D. Shen, G. Wu, and H. Suk, "Deep learning in medical image analysis," *Annu. Rev. Biomed. Eng.*, vol. 19, pp. 221–248, Jun. 2017.
[27] V. Badrinarayanan, A. Kendall, and R. Cipolla, "SegNet: A deep convolutional encoder-decoder architecture for image segmentation," *IEEE Trans. Pattern Anal. Mach. Intell.*, vol. 39, no. 12, pp. 2481–2495, Dec. 2017.
[28] J. Long, E. Shelhamer, and T. Darrell, "Fully convolutional networks for semantic segmentation," in *Proc. IEEE Conf. Comput. Vis. Pattern Recognit.*, Jun. 2015, pp. 3431–3440.
[29] E. Heiberg, J. Sjögren, M. Ugander, M. Carlsson, H. Engblom, and H. Arheden, "Design and validation of segment-freely available software for cardiovascular image analysis," *BMC Med. Imag.*, vol. 10, no. 1, p. 1, 2010.
[30] E. Heiberg, H. Engblom, J. Engvall, E. Hedström, M. Ugander, and H. Arheden, "Semi-automatic quantification of myocardial infarction from delayed contrast enhanced magnetic resonance imaging," *Scandin. Cardiovascular J.*, vol. 39, no. 5, pp. 267–275, 2005.
[31] L. Shao and H. Zhou, "Curve fitting with Bezier cubics," *Graph. Models Image Process.*, vol. 58, no. 3, pp. 223–232, 1996.
[32] *Evaluation of Cardiac MR Segmentation*. Accessed: Jul. 18, 2011. [Online]. Available: http://sourceforge.net/projects/cardiac-mr/files/
[33] P. Radau, Y. Lu, K. Connelly, G. Paul, A. J. Dick, and G. A. Wright, "Evaluation framework for algorithms segmenting short axis cardiac MRI," *Graph. Models Image Process.*, to be published.
[34] H. H. Chang, A. H. Zhuang, D. J. Valentino, and W. C. Chu, "Performance measure characterization for evaluating neuroimage segmentation algorithms," *NeuroImage*, vol. 47, no. 1, pp. 122–135, 2009.
[35] T. A. Ngo, Z. Lu, and G. Carneiro, "Combining deep learning and level set for the automated segmentation of the left ventricle of the heart from cardiac cine magnetic resonance," *Med. Image Anal.*, vol. 35, pp. 159–171, Jan. 2017.
[36] T. A. Ngo and G. Carneiro, "Fully automated non-rigid segmentation with distance regularized level set evolution initialized and constrained by deep-structured inference," in *Proc. IEEE Conf. Comput. Vis. Pattern Recognit.*, Jun. 2014, pp. 3118–3125.
[37] S. Queirós, D. Barbosa, B. Heyde, P. Morais, J. L. Vilaça, D. Friboulet, O. Bernard, and J. D'hooge, "Fast automatic myocardial segmentation in 4D cine CMR datasets," *Med. Image Anal.*, vol. 18, no. 7, pp. 1115–1131, 2014.
[38] C. Constantinidès, E. Roullot, M. Lefort, and F. Frouin, "Fully automated segmentation of the left ventricle applied to cine MR images: Description and results on a database of 45 subjects," in *Proc. Annu. Int. Conf. IEEE Eng. Med. Biol. Soc.*, Aug. 2012, pp. 3207–3210.
[39] L. Gupta and T. Sortrakul, "A Gaussian-mixture-based image segmentation algorithm," *Pattern Recognit.*, vol. 31, no. 3, pp. 315–325, 1998.
[40] N. Otsu, "A threshold selection method from gray-level histograms," *IEEE Trans. Syst., Man, Cybern.*, vol. SMC-9, no. 1, pp. 62–66, Jan. 1979.
[41] Z. Hou, Q. Hu, and W. L. Nowinski, "On minimum variance thresholding," *Pattern Recognit. Lett.*, vol. 27, no. 14, pp. 1732–1743, 2006.
[42] X. Xu, S. Xu, L. Jin, and E. Song, "Characteristic analysis of Otsu threshold and its applications," *Pattern Recognit. Lett.*, vol. 32, no. 7, pp. 956–961, 2011.
[43] A. Pednekar, U. Kurkure, R. Muthupillai, S. Flamm, and I. A. Kakadiaris, "Automated left ventricular segmentation in cardiac MRI," *IEEE Trans. Biomed. Eng.*, vol. 53, no. 7, pp. 1425–1428, Jul. 2006.

YIHUA LAN received the Ph.D. degree in computer science and technology from the Huazhong University of Science and Technology (HUST), in 2011, where he is currently a Postdoctoral Fellow with the School of Computer Science and Technology. He serves as an Associate Professor of computer science with the School of Computer and Information Technology, Nanyang Normal University, China. He holds the position of WoLong Scholar at Nanyang Normal University. His main research interests include cloud computing, machine learning, and computer-aided diagnosis.

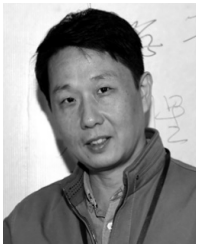

RENCHAO JIN received the M.S. and Ph.D. degrees in computer software and theory from the Huazhong University of Science and Technology (HUST), China, in 1989 and 1998, respectively, where he is currently a Professor with the School of Computer Science and Technology and the Key Laboratory of Education Ministry for Image Processing and Intelligence Control. His current research interests include artificial intelligence, computer vision, medical image processing, and medical image information analysis.